REVISION 6

Thermal Infrared and Raman Microspectroscopy of Moganite-bearing Rocks

Craig Hardgrove[1] and Deanne Rogers[1]

[1]Department of Geosciences, Stony Brook University, Stony Brook, NY

Abstract

We present the first thermal infrared reflectance spectral characterization of moganite and mixtures of moganite with microcrystalline quartz. We find that for relatively high (>50%) abundances of moganite, the absolute reflectance for samples is significantly reduced. Using microscopic-Raman (~1 μm/pixel) measurements, we estimate the moganite content for a variety of samples. We then compare Raman-derived moganite abundances with microscopic infrared reflectance (25 μm/pixel) spectra to determine the effects of increasing moganite abundance on thermal infrared spectra. We find that moganite is broadly spectrally similar to quartz with major reflectance maxima located between ~1030 and 1280 cm^{-1} and ~400 and 600 cm^{-1}; but there are characteristic differences in the peak shapes, peak center positions, and especially the relative peak reflectance magnitudes. For regions with high (>50%) moganite content, the relative magntitudes of the reflectance maxima at 1157 cm^{-1} and 1095 cm^{-1} (R_{1095}/R_{1157} band ratio) can be used to estimate the moganite content. This work demonstrates the utility of thermal infrared microspectroscopy in isolating phases that are intimately mixed in a sample, and has applications in planetary science, where constituent phases of quartz-rich sedimentary rocks can be identified using remote or in-situ thermal infrared spectroscopy.

Key words: Moganite, chert, microcrystalline quartz, silica, Raman spectroscopy, Infrared Spectroscopy, Microspectroscopy, Mars

Introduction

Moganite, a silica polymorph, is a microcrystalline mineral first discovered in ignimbrite flows on the island of Gran Canaria (Flörke et al., 1976, 1984). Later, several comprehensive studies have identified moganite in a variety of fibrous and granular microcrystalline quartz samples, suggesting moganite is present in many terrestrial microcrystalline quartz deposits (Heaney and Post, 1992; Godovikov et al., 1991). On Earth, moganite is typically intergrown with quartz in chert and chalcedony, which precipitates from silica-rich waters at temperatures characteristic of hydrothermal and diagenetic environments, and has been found as a weathering product on terrestrial volcanic rocks and in hydrothermally altered basalt veins (Flörke et al., 1982; Heaney and Post, 1992; Parthasarathy, 2001). Moganite also forms with microcrystalline quartz from diagenesis of opal (Knauth, 1994). On Mars, thermal infrared (TIR) emissivity data have been extensively acquired of the surface, by both Mars Exploration Rovers Spirit and Opportunity, using the Mini-TES (Miniature-Thermal Emission Spectrometer) instruments (Christensen et al. 2003), as well as the orbiting Mars Global Surveyor Thermal Emission Spectrometer (TES) (Christensen et al. 2001). TIR spectra collected from the Spirit rover's Mini-TES instrument were used to identify opaline silica, which is thought to have formed in a hydrothermal environment (Ruff et al., 2011). Quartz-bearing lithologies have been identified with TES data in craters found within Syrtis Major (Bandfield et al. 2004). As evidence for aqueous alteration and hydrothermal environments on Mars continues to grow (e.g. Bandfield, 2008; Ehlmann et al. 2009; Ehlmann et al. 2011), it is reasonable to determine whether moganite,

48 which can be used as a diagenetic indicator, would be detectible using instruments on current
49 Mars rovers or orbiters.
50
51 *Moganite*
52 A comprehensive discussion of the crystal structure of moganite, which is consistent with
53 space group *I2/a* and described as stacked, alternating layers of left and right-handed quartz, can
54 be found in Graetsch (1994a). Previous studies have shown that moganite is readily identifiable
55 using X-ray diffraction (Miehe and Graetsch, 1992), infrared absorption spectroscopy (Graetsch
56 et al., 1994b) and Raman spectroscopy (Kingma and Hemley, 1994). Studies of terrestrial
57 moganite abundances have revealed concentrations are higher in samples from arid
58 environments, suggesting the relative amounts of quartz and moganite within a given sample can
59 be used as an indicator of the environment subsequent to deposition (Heaney, 1995).
60 Experiments on moganite have determined that its rapid dissolution rate and high solubility
61 could be used to explain these observations (Petrovic et al., 1996; Gislason et al., 1997). On the
62 basis of these works, it was suggested that the absence of moganite within microcrystalline
63 quartz deposits is indicative of high water to rock ratios in the post-depositional environment. In
64 addition, variability in moganite content has been linked to macroscopic variations in color and
65 texture within a sample, indicating that variable moganite content may be linked to changing
66 environmental or depositional conditions (Kingma and Hemley, 1994).
67
68 Microcrystalline silica and moganite can precipitate directly from a silica-rich solution or
69 can form through the diagenesis of opal (Heaney, 1993). A typical diagenetic sequence of opal
70 is Opal A → Opal CT → microcrystalline (fibrous or granular) quartz (Knauth, 1994). The

identification of opal on Mars, therefore, suggests formation of microcrystalline quartz through one or both of these mechanisms. Recent studies have determined that the thermodynamic instability of moganite leads to its lack of preservation in rocks older than ~400 million years (Moxon and Rios, 2004). Given the terrestrial evidence that opal represents a diagenetically young form of quartz and moganite, and that moganite abundance can be used to constrain post-depositional environment, the identification of moganite on Mars using TIR spectroscopy may provide constraints on the timing of deposition and/or the post-depositional environment. Although moganite has not yet been identified on Mars, its formation is dependent upon the presence of iron in the fluid as well as high activity of alkalis and/or sulfates (Heaney and Post, 1992; Heaney, 1995; McLaren and Pitkethly, 1982). In addition Al^{3+} can act as a catalyst in the formation of agate incorporating moganite (Story et al., 2010; Moore, et al., 2010; Wang and Merino, 1990). In-situ and orbital observations have provided widespread evidence for the presence of iron-rich fluids in diagenetic and hydrothermal environments (Ming et al., 2008) through detections of Fe-bearing sulfates (Squyres, et al. 2004; Wray, et al., 2011) and phyllosilicates (Poulet, et al. 2005; Bibring, et al. 2006); Al-phyllosilicates are less common but still present (Noe Dobrea, et al. 2010). These observations suggest that conditions may have been appropriate on Mars for moganite to form.

A study of the thermal infrared properties of opaline silica and silica polymorphs was presented by Michalski et al., (2003), however, that study did not include moganite. Here, we present the first thermal infrared (TIR, ~6-25 μm) reflectance spectrum of moganite, and we quantify the effects of moganite abundance on infrared reflectance spectra of microcrystalline quartz. Because TIR bidirectional reflectance measurements of specular surfaces can be related

to emissivity using Kirchoff's law (ε=1-R) (e.g., Nicodemus, 1965; Salisbury, 1993), the spectra presented here can be converted and directly compared to emissivity spectra of quartz-bearing samples.

Methods

Overview

Previous work by Götze et al., (1998) showed that moganite abundances in microcrystalline quartz could be obtained using Raman spectroscopy. However, differences between the Raman- and X-ray Diffraction (XRD)-derived moganite abundances were found. These differences can be attributed to the short-range order of moganite within the sample. If moganite is present only as nano-scale lamellae, then the absence of a coherent Bragg scattering lattice domain leads to an underestimate of moganite abundance using XRD (Götze et al., 1998). Raman spectroscopy, however, is sensitive to lattice vibrations and will be sensitive to moganite on the unit cell scale. Moganite abundances as derived using Raman spectroscopy, therefore, place an upper limit on the amount of moganite within a given sample. We expect that infrared reflectance spectroscopy, which is also sensitive to the fundamental vibrational frequencies of the lattice, will likewise be sensitive to moganite abundances on the nano-scale. Building upon previous work, we first identified the moganite contents within a suite of microcrystalline quartz samples using Raman spectroscopy, following similar methods to those described by Götze et al., (1998). We used the 501 Δcm^{-1} peak to identify the presence of moganite within a sample while the 465 Δcm^{-1} peak is used to identify regions of microcrystalline quartz. Thus, the ratio of the areas of the 501 and 465 Δcm^{-1} peaks, as measured above the background, can be used to determine the moganite content (Götze et al., 1998). From the calibration data presented by

Götze et al., we derive two best-fit curves to relate the Raman band integral ratios to moganite abundances. We use an exponential curve (R^2 value of 0.965) to fit their calibration data for Raman-derived band integral ratios higher than 35, while a polynomial fit (R^2 value of 0.999) is more appropriate for band integral ratios lower than 35.

We then used the Raman band integral ratio to moganite content calibration curve defined in Götze et al., (1998) to relate our own band ratios derived from thermal infrared spectra to moganite contents. Recent work by Schmidt et al., (2012) has shown that heating can reduce the intensity of the moganite peak in chalcedony, which indicates that for heated samples moganite content will be underestimated by the Götze et al. calibration curve. Therefore, for chalcedony samples, our cited moganite content values represent a minimum moganite content. The diversity of samples chosen for our study, which includes several cherts, gives confidence that the correlated trends in spectral parameters are consistent with moganite content.

Once moganite contents were determined, we analyzed the same samples and locations using a microscopic Fourier Transform Infrared (FTIR) spectrometer. Microspectroscopy is well-suited for analysis of these samples because the moganite is commonly intimately mixed with α-quartz within the microcrystalline samples. Using these data, we present the TIR reflectance spectra for samples containing variables amounts of moganite and microcrystalline quartz. Correlated TIR spectra and Raman-derived moganite contents are then used to demonstrate how TIR reflectance features can be used to infer the moganite abundance within a sample.

140 *Sample Descriptions*

141 Because fibrous and non-fibrous microcrystalline quartz can contain moganite, we have
142 selected examples of both from a variety of locations. Samples were acquired from the National
143 Museum of Natural History and the Stony Brook Department of Geosciences mineral
144 collections. Table 1 shows a list of sample names and brief petrographic descriptions of each.
145 As our reference moganite sample, we use a well-studied specimen from the type locality on
146 Gran Canaria (National Museum of Natural History sample number *NMH-168357*). This sample
147 is composed primarily of a homogenous gray chert, surrounded by a white powdery material
148 (Sample Name: "moganite"). As previously reported, the white powdery rims have high
149 concentrations of moganite as determined by bulk diffraction and Raman measurements (Heaney
150 and Post, 1992; Miehe and Graetsch, 1992). Other samples include two banded iron formation
151 samples ("BIF", "Jaspilite"), two chalcedony samples ("Chalcedony", "Rose Chalcedony"), and
152 two non-fibrous chert samples ("Chert", "Novaculite"). Each sample was prepared as a thin
153 section (polished to 1 μm, 30 μm thickness) for petrographic and subsequent micro-Raman and
154 micro-FTIR analyses. Samples were examined petrographically to determine the degree of
155 homogeneity in texture and mineralogy. Samples that are homogeneous on the scale of the field
156 of view for both the Raman (~100's of microns) and FTIR (~centimeters) optics were preferred,
157 as this ensured consistency in the spatial locations for measurements acquired on both
158 instruments. Figure 1 shows petrographic images (in cross-polarized light) for each sample
159 studied.

160

161 *FTIR and Raman Instrumentation*

Micro-Raman and micro-FTIR analyses were conducted at the Vibrational Spectroscopy Laboratory (VSL) in the Department of Geosciences at Stony Brook University. For micro-FTIR analyses, we use a Nicolet iN10MX FTIR microscope equipped with a liquid nitrogen cooled Mercury Cadmium Telluride (MCT) array detector capable of acquiring hyperspectral image cubes between 7000 and 715 cm^{-1}; in point-sampling mode, a spectral range of 450-4000 cm^{-1} may be achieved. Spectra were background corrected using a gold plate, with the system purged of CO_2, and acquired in mapping mode to cover a ~0.5 cm by ~0.5 cm area with individual pixel sizes of 25 microns. The total integration time for each pixel was ~0.1 s, resulting in low noise and clearly distinguishable peaks. Our reflectance measurements are of polished surfaces with roughness <1μm, thereby producing a specular surface for the TIR wavelengths of interest. Under these conditions, measured reflectance spectra can also be approximated as emissivity via Kirchoff's law (e.g., Nicodemus, 1965; Salisbury, 1993).

Raman analyses were conducted using a WiTEC alpha300R confocal Raman microscope system equipped with a frequency doubled 532 nm Nd:YAG excitation laser. The nominal laser power is 50 mW at 532 nm. The Raman imaging spectrometer acquires spectra from 3500-150 Δcm^{-1} and is equipped with multiple objective lenses, ranging from 4X to 100X magnification, enabling spatial resolutions between several microns and 250 nm/pixel. The confocal Raman system utilizes an ultra-high throughput screening (UHTS) 300 f/4, 300 mm focal length imaging spectrometer with a motorized double grating turret equipped with 600 and 1800 groove/mm gratings, enabling spectral resolution of ~3 and ~1.3 cm^{-1} respectively.

The general homogeneity in texture of some samples combined with the significantly higher spatial resolution of the Raman imaging system (250 nm/pixel to ~2 μm/pixel) made comparisons with micro-FTIR spectra (25 μm/pixel) challenging. To accommodate this issue, when possible we identified spatial regions of our samples having distinct textures that could readily be identified using both the Raman (with low magnification) and micro-FTIR imaging systems. The micro-FTIR was used to acquire spectral data for a large enough region (typically with a field of view of ~2000 - 5000 μm) to encompass the texturally distinct feature. The same region was identified using low magnification optics on the Raman imaging system; however, for data acquisition (< 1 μm/pixel), spectra were acquired with high magnification for between 10-20 spots within each textural domain. All averaged micro-FTIR and Raman spectra are for a single texture, whose location was identified using spatial relationships established during petrographic analyses. For micro-FTIR spectra, we averaged spectra for pixels around which the 10-20 Raman measurements were acquired. These regions are typically defined by the textural boundaries of the sample itself, or in the case of homogeneous samples, are defined by the slide itself (where the slide corners were used for reference). Averaged micro-FTIR spectra typically consist of between 10-12 pixels, which corresponds to a spatial region between 250 - 300 μm. The 10-20 Raman spots (< 1 μm/pixel) uniformly sample the entire 250-300 μm region where the micro-FTIR spectra were extracted.

Results

Figure 1 shows the textural diversity as well as approximate locations for Raman and micro-FTIR measurements on the microcrystalline samples chosen in our study. Where textural differences related to moganite content were present, multiple sets of measurements were

acquired on a single sample and the locations of subsequent sets of measurements are labeled with a dashed circle in Fig. 1. Similar to Götze et al., (1998), we found that moganite abundances did not vary significantly within homogeneous textures (see "Moganite" and "Moganite, Mixture" in Figure 1); however, moganite abundances do vary across textural boundaries (see "Rose Chalcedony" in Figure 1). Raman spectra are presented in Figure 2 for each sample and texture, in order of decreasing moganite content from top to bottom. Table 2 shows the Raman band integral ratios for moganite and quartz, as derived from the Raman spectra presented in Figure 2. For reference, we also present the moganite content as derived using the methods of Götze et al., (1998). The Raman spectrum was analyzed using the Arizona State University's RRUFF (http://www.rruff.info) database to detect the presence of any other phases that might be present in the samples. Specifically, we found no evidence for opaline silica, and locations of detailed analyses were dominated by quartz and moganite peaks. Corresponding micro-FTIR spectra for each sample are presented in Figure 3a.

Figure 3a shows that, as expected, moganite has similar spectral characteristics to quartz. The primary differences are manifested as an overall lower absolute reflectance for moganite across the spectral range, as well as a lowered reflectance associated with the higher frequency restrahlen peak (in moganite, centered at ~1157 cm^{-1}) relative to the lower frequency restrahlen peak (in moganite, centered at ~1095 cm^{-1}). With increasing moganite abundance, narrowing and a shift of the lower frequency quartz restrahlen peak centered near ~1125 cm^{-1} to ~1095 cm^{-1} are also observed (Figure 3a). For comparison of sample "Moganite" and pure microcrystalline α-quartz, we also present the spectral features for an extended spectral range (~400 cm^{1} to 2200 cm^{1}) in Figure 3b.

230

231 The spectral features in both quartz and moganite between ~1030-1280 cm^{-1} are due to
232 Si-O stretching modes within the silica tetrahedra (e.g. Lippincott et al. 1958). Because the
233 fourfold Si coordination is preserved in both phases, the TIR spectra are broadly similar (e.g.,
234 White and Roy, 1964). Rather, the orientations of tetrahedra within the unit cell are likely the
235 dominant factors controlling the differences in this spectral region. Though moganite has a lower
236 symmetry than quartz (Miehe and Graetsch, 1992) the number of IR-active optical modes is 12
237 for both phases (Scott and Porto, 1967; Kingma and Hemley, 1994; Heaney et al. 2007). This,
238 combined with preservation of coordination and bond type (e.g., small structural changes
239 between polymorphs), further accounts for the remarkable TIR spectral similarities between
240 them.

241

242 Although the most distinct differences between moganite and quartz are found between
243 ~1030-1280 cm^{-1}, there is a subtle difference in the shape of the peak related to Si-O bending
244 vibrations between ~400-600 cm^{-1}, including a new, small peak near ~550 cm^{-1}. These
245 differences are likely related to the change from 6-ring structure to 4-, 6-, and 8-ring structure
246 between quartz and moganite (Kingma and Hemley, 1994).

247

248 The characteristic difference in reflectance magnitude at ~1095 cm^{-1} relative to ~1157
249 cm^{-1} in moganite can be parameterized with a ratio of the reflectance values at these frequencies
250 (hereafter, "R_{1095}/R_{1157}"). Figure 4 shows the R_{1095}/R_{1157} parameter for each sample plotted with
251 the Raman-derived moganite content. Figure 5 shows the R_{1095}/R_{1157} band parameter map (25
252 μm/pixel) for each sample studied. These maps illustrate the effectiveness in using this

parameter to identify moganite-rich areas in micro-FTIR images. In general, our data show that with decreasing moganite content, R_{1095}/R_{1157} ratio values decrease. Samples where moganite was detected have ratio values between 1.38 and 1.93, whereas samples with no moganite have values between 1.30 and 1.42. For the two moganite-bearing samples where moganite is present below 50%, the ratio values are within or very close to the range of the moganite free samples. In addition, the band parameter for the "BIF" sample of 1.42 (which Raman spectra revealed contains no moganite) and the "Rose Chalcedony, moganite" sample of 1.43 (which contains ~50% moganite) are not significantly different. This suggests that the R_{1095}/R_{1157} band parameter is not sensitive to moganite abundance below approximately 50% by volume. This is further evidenced by the strong reduction (of ~50%) in absolute reflectance for the "moganite" sample relative to both microcrystalline quartz as well as a mixture containing primarily moganite (~90%) and microcrystalline quartz (Figure 3b). This indicates that when mixed with microcrystalline quartz, moganite does not contribute as significantly to the overall infrared spectrum. This results in a lack of sensitivity to moganite abundance for the R_{1095}/R_{1157} parameter for samples with moganite abundance less than ~50%.

Discussion and Conclusions

We have shown how moganite can be identified using micro-FTIR reflectance spectroscopy. If present in abundances > ~50%, a distinct increase in the TIR reflectance at ~1095 cm^{-1} relative to ~1157 cm^{-1} can be observed. Abundances of moganite can be estimated using the Gotze et al. calibration curve and the R_{1095}/R_{1157} band ratio if the ratio is relatively high (> 1.45). Relatively low values of the R_{1095}/R_{1157} band ratio (< 1.45) may indicate either low abundance (less than 50%) or no moganite within the sample. In either case, the R_{1095}/R_{1157} band

ratio may be used to discriminate between samples with relatively high and low moganite content.

Our results demonstrate that the presence of moganite may be identified using thermal infrared reflectance techniques. Though our study was conducted using prepared and polished samples, the effects of surface roughness may play a more dominant role in the overall TIR spectrum of natural (unpolished) microcrystalline quartz surfaces (Hardgrove and Rogers, 2012), and will be the subject of future work. However, we can conclude that for surfaces that are smooth at ~1 μm scales, relative moganite abundances will have the largest influence on the R_{1095}/R_{1157} ratio within the restrahlen bands of quartz in the thermal infrared. Because the relative depths and positions of spectral absorption features obtained using microspectroscopy can be readily compared to those obtained using macrospectroscopic techniques (Klima and Pieters, 2006), microspectroscopy is a useful tool for obtaining spectral measurements of phases that are important in nature but that primarily occur in intimate mixtures or as fracture/vein-filling material. The distribution of moganite within microcrystalline quartz, which will be homogenous when viewed on a macro-scale (millimeters to centimeters), actually varies on a micro-scale (μm) and, therefore, provides an excellent example of the value of microspectroscopy in unraveling the geologic history of planetary surfaces. Microspectral techniques may play an important role in the future of planetary exploration, as a visible light micro-fluorescence spectrometer MArs Hand Lens Imager (MAHLI), with a spatial resolution of 15 μm, is already en-route to Mars on the Mars Science Laboratory rover (Edgett et al., 2005). Micro-infrared reflectance or emission spectroscopy would be complementary to this type of

instrument, as textural, color and albedo boundaries could be correlated with variations in mineralogic abundances on the micron scale.

Acknowledgments

We would like to thank the NASA Mars Fundamental Research Program (NNX09AL22G) and the National Science Foundation's Major Research Instrumentation program (EAR-0922827). We also wish to thank two anonymous reviewers for their informed and helpful comments that greatly strengthened this manuscript. Some samples were graciously provided by the Smithsonian National Museum of Natural History. In addition, this work could not have been completed without the help of Tim Glotch, Ben McKeeby, Troy Rasbury, Cara Thompson, and Bill Woerner.

References

Bandfield, J. L., Hamilton, V.E., Christensen, P.R., McSween Jr., H.Y. (2004) Identification of quartzofeldspathic materials on Mars. Journal of Geophysical Research, 109, E10009.

Bandfield, J. L. (2008) High-silica deposits of an aqueous origin in western Hellas Basin, Mars. Geophysical Research Letters, 35, L12205.

Bibring, J.P., Langevin, Y., Mustard, J.F., Poulet, F., Arvidson, R., Gendrin, A., Gondet, B., Mangold, N., Pinet, P., Forget, F., the OMEGA team. (2006) Global Mineralogical and Aqueous Mars History Derived from OMEGA/Mars Express Data. Science, 312, 400-404.

Christensen, P.R., Bandfield, J.L., Hamilton, V.E., Ruff, S.W., Kieffer, H.H., Titus, T.N., Malin, M.C., Morris, R.V., Lane, M.D., Clark, R.L., Jakosky, B.M., Mellon, M.T., Pearl, J.C., Conrath, B.J., Smith, M.D., Clancy, R.T., Kuzmin, R.O., Roush, T., Mehall, G.L., Gorelick, N., Bender, K., Murray, K., Dason, S., Greene, E., Silverman, S., Greenfield, M. (2001) Mars Global Surveyor Thermal Emission Spectrometer experiment: Investigation description and surface science results. Journal of Geophysical Research, 106, E10, 23823-23871.

Christensen, P.R., Mehall, G.L., Silverman, S.H., Anwar, S., Cannon, G., Gorelick, N., Kheen, R., Tourville, T., Bates, D., Ferry, S., Fortuna, T., Jeffryes, J., O'Donnell, W., Peralta, R., Wolverton, T., Blaney, D., Denise, R., Rademacher, J., Morris, R.V., Squyres, S. (2003) Miniature Thermal Emission Spectrometer for the Mars Exploration Rovers. Journal of Geophysical Research, 108, 8064.

Ehlmann, B.L., Mustard, J.F., Swayze, G.A., Clark, R.N., Bishop, J.L., Poulet, F., Des Marais, D.J., Roach, L.H., Milliken, R.E., Wray, J.J., Barnouin-Jha, O., Murchie, S.L (2009) Identification of hydrated silicate minerals on Mars using MRO-CRISM: Geologic context near Nili Fossae and implications for aqueous alteration. Journal of Geophysical Research, 114, E00D08.

Edgett, K., Bell III, J.F., Herkenhoff, K.E., Heydari, E., Kah, L.C., Minitti, M.E., Olson, T.S., Rowland, S.K., Schieber, J., Sullivan, R.J., Yingst, R.A., Ravine, M.A., Caplinger, M.A., Maki,

344 J.N. (2005) The Mars Hand Lends Imager (MAHLI) for the 2009 Mars Science Laboratory.
345 Lunar and Planetary Science Conference, XXXVI, Abst. 1170.
346
347 Flörke, O.W., Jones J. B., and Schmincke H. U. (1976) A new microcrystalline silica from Gran
348 Canaria. Zeitschrift für Kristallographie, 143, 156-165.
349
350 Flörke, O.W., Kohlerherbertz, B., Langer, K., Tönges, I. (1982) Water in Microcystalline Quartz
351 of Volcanic Origin – Agates. Contributions to Mineralogy and Petrology, 80, 324-333.
352
353 Flörke, O.W., Flörke U., and Giese U. (1984) Moganite. A new microcrystalline silica-mineral.
354 Neues Jahrbuch für Mineralogie Abhandlungen, 149, 325-336.
355
356 Gislason S.R., Heany P.J., Oelkers E.H., Schott J. (1997) Kinetic and thermodynamic properties
357 of moganite, a novel silica polymorph. Geochimica et Cosmochimica Acta, 61, 1193-1204.
358
359 Glotch, T.D., Rossman, G.R., Aharonson, O. (2007) Mid-infrared (5-100 um) reflectance spectra
360 and optical constants of ten phyllosilicate minerals. Icarus, 192, 605-622.
361
362 Godovikov, A.A., Nenasheve, S.N., Pavlyuchenko, V S., and Ripinen, O.I. (l99l) New finds of
363 lutecite. Doklady Akademie Nauk, SSSR, 320, 428-433 (in Russian).
364

Götze, J., Nasdala, L., Kleeberg, R., Wenzel, M. (1998) Occurrence and distribution of "moganite" in agate/chalcedony: a combined micro-Raman, Rietveld, and cathodoluminescence study. Contributions to Mineralogy and Petrology, 133, 96-105.

Graetsch, H., (1994a), Structure of Opaline and Microcrystalline Silica. Reviews in Mineralogy and Geochemistry, 29, 209-232.

Graetsch, H., Gles, H., Topalovic, I. (1994b), NMR, XRD and IR study of microcrystalline opals. Physics and Chemistry of Minerals, 21, 166-175.

Hardgrove, C. and Rogers, A.D., (2012) Thermal Infrared Spectra of Microcrystalline Sedimentary Phases: Effects of Natural Surface Roughness on Spectral Feature Shape. 43rd Lunar and Planetary Science Conference. Abst. 1675.

Heaney, P. J. (1993) A proposed mechanism for the growth of chalcedony. Contributions to Mineralogy and Petrology, 115, 66-74.

Heaney P. J. (1995) Moganite as an indicator for vanished evaporites: A testament reborn? Journal of Sedimentary Research, A65, 633-638.

Heaney, P. J., McKeown, D. A., and Post, J. E. (2007) Anomalous behavior at the I2/a to Imab phase transition in SiO_2-moganite: An analysis using hard-mode Raman spectroscopy. American Mineralogist, 92, 631-639.

Heaney P. J. and Post J. E. (1992) The widespread distribution of a novel silica polymorph in microcrystalline quartz varieties. Science, 255, 441-443.

Kingma, K.J. and Hemley, R.J. (1994) Raman spectroscopic study of microcrystalline silica. American Mineralogist, 79, 269-273.

Knauth, P. (1994) Petrogenesis of Chert. Reviews in Mineralogy and Geochemistry, 29, 233-258.

Lippincott, E. R., Vanvalkenburg, A., Weir, C. E., and Bunting, E. N. (1958) Infrared Studies on Polymorphs of Silicon Dioxide and Germanium Dioxide. Journal of Research of the National Bureau of Standards, 61, 61-70.

McLaren, A.C., and Pitkethly, D.R. (1982), The twinning microstructure and growth of amethyst quartz. Physica Status Solidi, 31, 723-737.

Michalski, J.R., Kraft, M.D., Diedrich, T., Sharp, T.G., Christensen, P.R. (2003) Thermal emission spectroscopy of the silica polymorphs and considerations for remote sensing of Mars. Geophysical Research Letters, 30, 2008.

Miehe G. and Graetsch H. (1992) Crystal structure of moganite: A new structure type for silica. European Journal of Mineralogy, 4, 693-706.

Ming, D. W., Gellert, R., Morris, R.V., Arvidson, R.E., Brückner, J., Clark, B.C., Cohen, B.A., d'Uston, C., Economou, T., Fleischer, I., Klingelhöfer, G., McCoy, T.J., Mittlefehldt, D.W., Schmidt, M.E., Schröder, C., Squyres, S.W., Tréguier, E., Yen, A.S., Zipfel, J. (2008), Geochemical properties of rocks and soils in Gusev crater, Mars: Results of the Alpha Particle X-Ray Spectrometer from Cumberland Ridge to Home Plate. Journal of Geophysical Research, 113, E12S39.

Moxon, T. and Rios, S. (2004) Moganite and water content as a function of age in agate: an XRD and thermogravimetric study. European Journal of Mineralogy 16, 269-278.

Moore, J.M., Bullock, M.A., Newsom, H., Nelson, M. (2010) Laboratory simulations of Mars evaporite geochemistry. Journal of Geophysical Research, 115, E06009.

Nicodemus, F.E., (1965) Directional Reflectance and Emissivity of an Opaque Surface. Applied Optics, 4, 767-773.

Noe Dobrea, E.Z, Bishop, J.L., McKeown, N.K., Fu, R., Rossi, C.M., Michalski, J.R., Heinlein, C., Hanus, V., Poulet, F., Mustard, R.J.F., Murchie, S., McEwen, A.S., Swayze, G., Bibring, J.P., Malaret, E., Hash, C. (2010) Mineralogy and stratigraphy of phyllosilicate-bearing and dark mantling units in the greater Mawrth Vallis/west Arabia Terra area: Constraints on geological origin. Journal of Geophysical Research, 115, E00D19.

434 Parthasarathy, G., and Kunwar, A.C. (2001) Occurrence of moganite-rich chalcedony in Deccan
435 flood basalts, Killari, Maharahtra, India. European Journal of Mineralogy, 13, 127-134.
436
437 Petrovic, I. Heaney, P.J., Navrotsky, A., (1996) Thermochemistry of the new silica polymorph
438 moganite. Physics and Chemistry of Minerals, 23, 119-126.
439
440 Poulet, F., Bibring, J., Mustard, J., Gendren, A., Mangold, N., Langevin, Y., Arvidson, R.E.,
441 Gondet, B., Gomez, C. (2005) Phyllosilicates on Mars and implications for early martian
442 climate. Nature, 438, 623-627.
443
444 Rodgers, K.A. and Cressey, G., (2001) The occurrence, detection and significance of moganite
445 (SiO_2) among some silica sinters. Mineralogical Magazine, 65, 157-167.
446
447 Ruff, S.W., Farmer, J.D., Calvin, W.M., Herkenhoff, K.E., Johnson, J.R., Morris, R.V., Rice,
448 M.S., Arvidson, R.E., Bell III, J.F., Christensen, P.R., Squyres, S.W. (2011) Characteristics,
449 distribution, origin, and significance of opaline silica observed by the Spirit rover in Gusev
450 crater, Mars. Journal of Geophysical Research, 116, E00F23.
451
452 Salisbury, J. W. (1993) Mid-infrared spectroscopy: Laboratory data, in Remote Geochemical
453 Analysis: Elemental and Mineralogical Composition, edited by C. M. Pieters and P. A. J.
454 Englert. Cambridge University Press, New York, 79 – 98.
455

456 Schmidt, P. (2012) A hitherto unrecognised band in the Raman spectra of silica rocks: influence
457 of hydroxylated Si–O bonds (silanole) on the Raman moganite band in chalcedony and flint
458 (SiO_2). Physics and Chemistry of Minerals, 39, 455-464.
459
460 Scott, J. F., and Porto, S. P. S. (1967) Longitudinal And Transverse Optical Lattice Vibrations In
461 Quartz. Physical Review, 161, 903-910.
462
463 Squyres, S.W. (2004) In situ evidence for an ancient aqueous environment at Meridiani Planum,
464 Mars. Science, 306, 1709-1714.
465
466 Story, S., Bowen, B.B., Benison, K.C., Schulze, D.G. (2010) Authigenic phyllosilicates in
467 modern acid saline lake sediments and implications for Mars. Journal of Geophysical Research,
468 115, E12012.
469
470 Wang, Y. and Merino, E. (1990) Self-organizational origin of agates: Banding, fiber twisting,
471 composition and dynamic crystallization model. Geochemica et Cosmochimica Acta, 54, 1627-
472 1638.
473
474 White, W. B., and Roy, R. (1964), Infrared Spectra-Crystal Structure Correlations: II.
475 Comparison Of Simple Polymorphic Minerals. American Mineralogist, 49, 1670-1687.
476
477 Wray, J.J., Milliken, R.E., Dundas, C.M., Swayze, G.A., Andrews-Hanna, J.C., Baldridge, A.M.,
478 Chojnacki, M., Bishop, J.L., Ehlmann, B.L., Murchie, S.L., Clark, R.N., Seelos, F.P., Tornabene,

L.L., Squyres, S.W. (2011) Columbus crater and other possible groundwater-fed paleolakes of Tera Sirenum, Mars. Journal of Geophysical Research, 116, E01001.

Figure Captions

Figure 1: Petrographic images for each sample and the approximate locations for micro-FTIR and micro-Raman measurements. Circles indicate locations of spectral measurements. Where dashed circles are present, multiple sets of measurements were made for that sample. The samples are: A) Moganite, (solid); Moganite, mixture (dashed), B) Rose Chalcedony, moganite (solid); Rose Chalcedony, no moganite (dashed), C) Chalcedony (solid), D) Chert, E) Novaculite, F) BIF (acquired in reflected light) and G) Jaspilite (acquired in reflected light).

Figure 2*:* Raman spectra for samples in order of decreasing moganite content (top to bottom). The band integral ratio of the moganite to quartz peak (501/465 Δcm^{-1}) was used to characterize the moganite content for various sections of each sample.

Figure 3: *a)* FTIR spectra for each sample, showing the change in quartz absorption band shapes for decreasing moganite content (from top to bottom). Dashed vertical lines mark the locations of the 1095 and 1157 cm^{-1} bands. The band ratio of R_{1095}/R_{1157} is sensitive to the abundance of moganite within each region studied on the sample. Spectra are normalized to the same spectral contrast so that differences in spectral shape may be readily compared. *b)* Unnormalized thermal infrared spectra for selected samples "Moganite" which contains ~99% moganite, "Moganite, mixture" which contains ~79% moganite and moganite-free quartz, "Macroquartz" which

contains no moganite. Dashed vertical lines mark the locations of the 1095 and 1157 cm^{-1} bands. Spectra were acquired from a single ~200 μm by ~200 μm spot on each sample. A room temperature detector was used, with a longer integration time to capture the infrared spectrum from 400-700 cm-1. These spectra are presented unnormalized to show the strong reduction in absolute reflectance for moganite-rich textures. This reduction indicates that the R_{1095}/R_{1157} band parameter will not be sensitive to moganite content for samples with less than ~50% moganite."

Figure 4: Moganite content with corresponding FTIR-derived R_{1095}/R_{1157} band parameter for all samples. Moganite content decreases from top to bottom. Comparing the R_{1095}/R_{1157} values with the moganite abundances determined from corresponding Raman-derived band integral ratios, we conclude that the R_{1095}/R_{1157} band parameter is not sensitive to moganite abundance below ~50%. This is evidenced by a similarity in band parameters for samples containing less than 50% moganite and samples with no moganite. This effect is due to the low absolute reflectance of moganite relative to quartz, which reduces moganite's contribution to infrared spectra when mixed with quartz.

Figure 5: FTIR-derived R_{1095}/R_{1157} ratio maps for each sample, showing the distribution of moganite abundances. Circles, approximately 300 μm in diameter, denote the locations for each measurement, which correspond to locations shown in Figure 1.

Table 1

Sample Names, Petrographic Description, Sample Locations

Sample Name	Petrographic Description	Sample Location
Moganite, powder	Moganite-rich powerdy material lining massive granular chert. Moganite appears as a white powder under visible light, and dark in plane and cross polarized light.	Gran Canaria, Canary Islands
Moganite, mixture	Massive granular chert mixed with moganite. This massive chert is lined by moganite-rich powerdy material.	Gran Canaria, Canary Islands
Chalcedony	Fibrous microcrystalline silica, with scattered chalcedony nodules.	Mexico
Rose Chalcedony, moganite	Parabolic chalcedony with rythmic extinction. This moganite-bearing chalcedony forms a wall lining megaquartz with interstitial chalcedony.	Mexico
Rose Chalcedony, no moganite	Chalcedony surrounded by megaquartz, indicating microquartz growth into microcavities and fractures	Mexico

Chert	Silicified limestone with granular chert with replacement chalcedony nodules	Mississippian Lake Valley, Sacramento Mtns., New Mexico
Novaculite	Massive granular chert with trace TiO_2	Ouachita Mountains, Arkansas
BIF	Alternating layers composed primarily of 1) major component of gray crystalline hematite with minor granular chert and 2) major component of granular chert with minor red crystalline hematite. Fine laminations of gray hematite and chert frequently appear within massive red crystalline hematite layers.	Minnesota
Jaspilite	Similar petrography to BIF with undulating layers of red and gray hematite.	Ishpeming, Michigan
Macroquartz	Quartz crystal with undulous extinction, bounded by massive potassium feldspar crystals (sampled from granite)	-

Table 2

Sample Name, Raman Band Ratios, Raman-Derived Moganite Content, FTIR

Sample Name	Raman Band Integral Ratio I_{501}/I_{465}	Raman-derived Moganite Content [wt.%]**	Reflectance Band Ratio R_{1095}/R_{1150}***
Moganite, powder	4.57	99	1.93
Moganite, mixture	0.80	79	1.73
Chalcedony	0.33	68	1.61
Rose Chalcedony, moganite	0.16	45	1.43
Chert	0.07	28	1.38
Rose Chalcedony, no moganite	-	0	1.30
Novaculite	-	0	1.33
Jaspilite	-	0	1.33
BIF	-	0	1.42
Macroquartz	-	0	1.34

**Derived using methods described in Gotze et al., 1998

***We estimate that the measurement error is likely less than 3%, which results in a relative error of 0.04 on the Reflectance Band Ratio. This is based on measurement repeatability determined by Glotch et al. (2007) for a similar reflectance instrument and specular surfaces

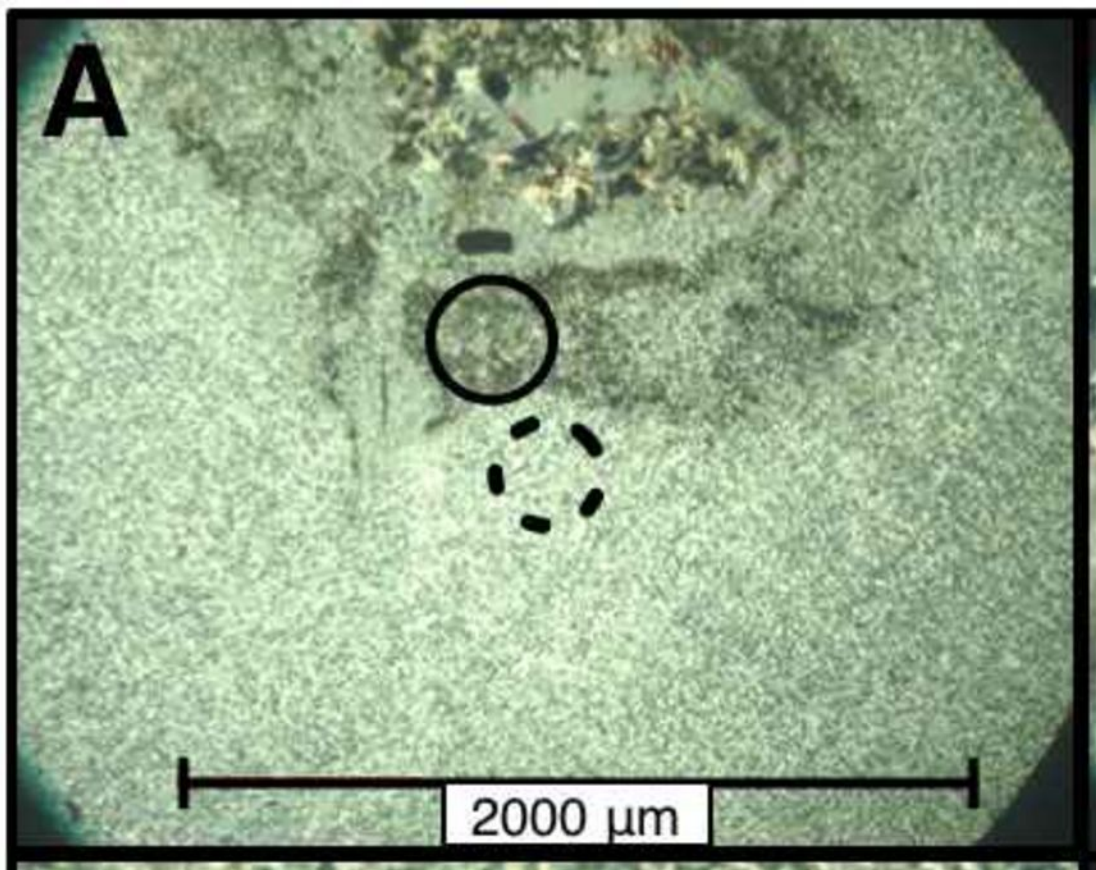

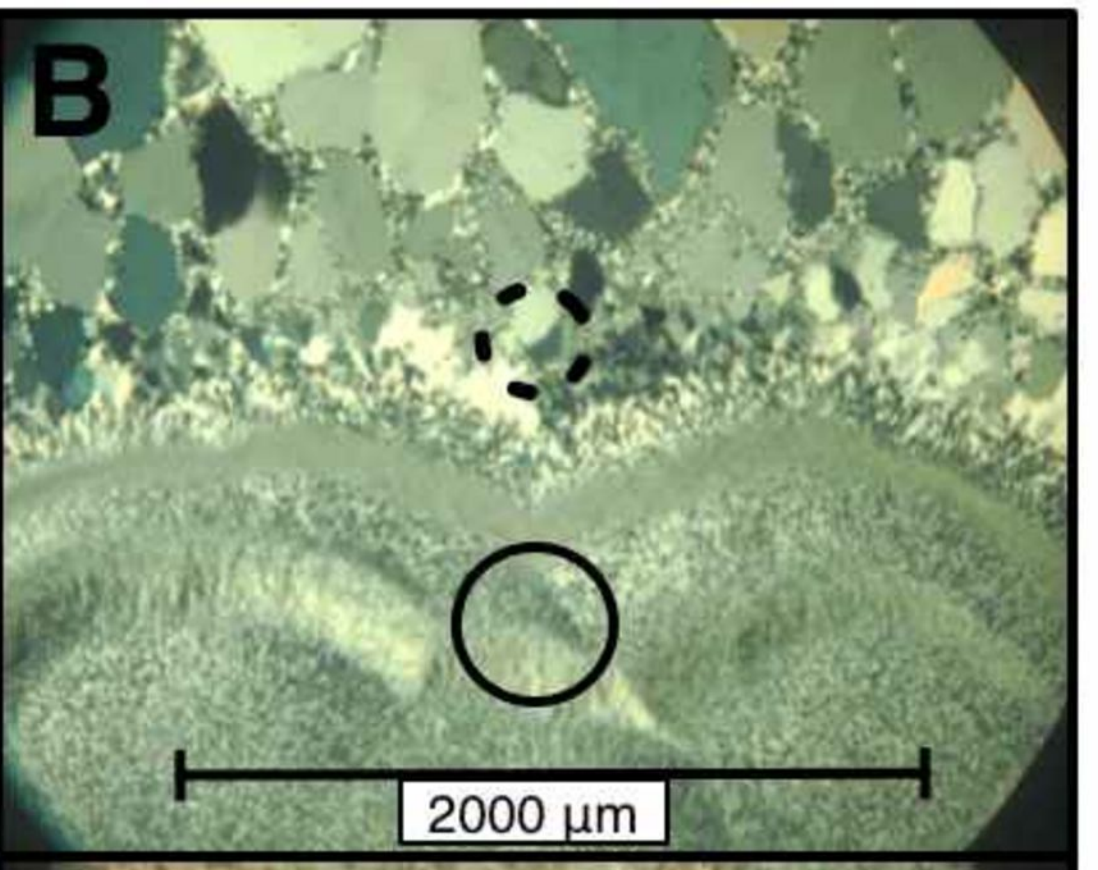

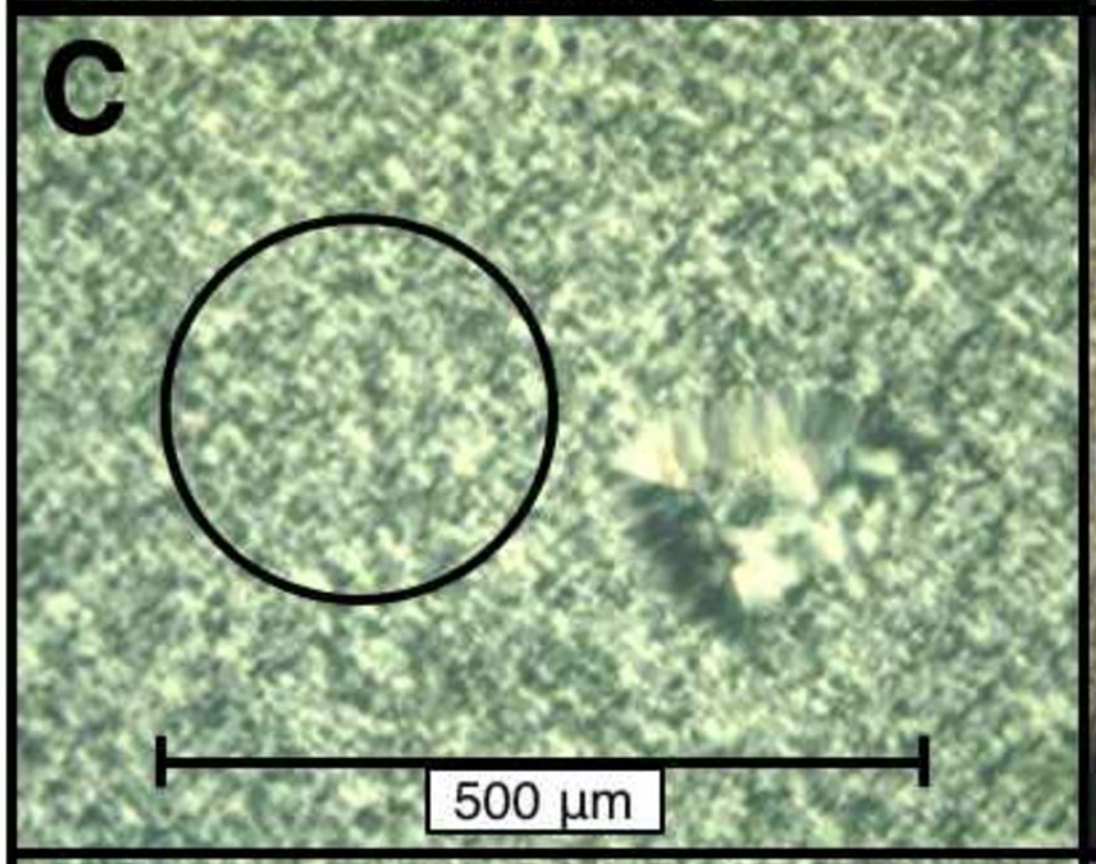

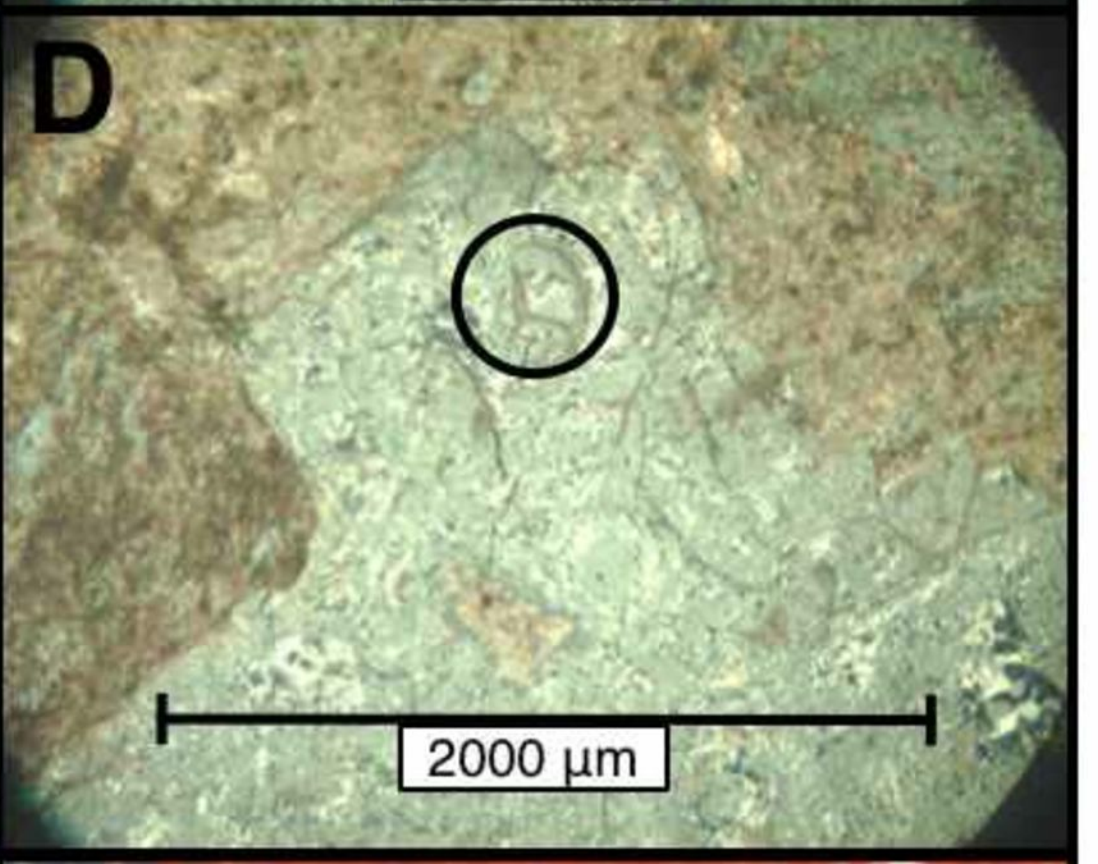

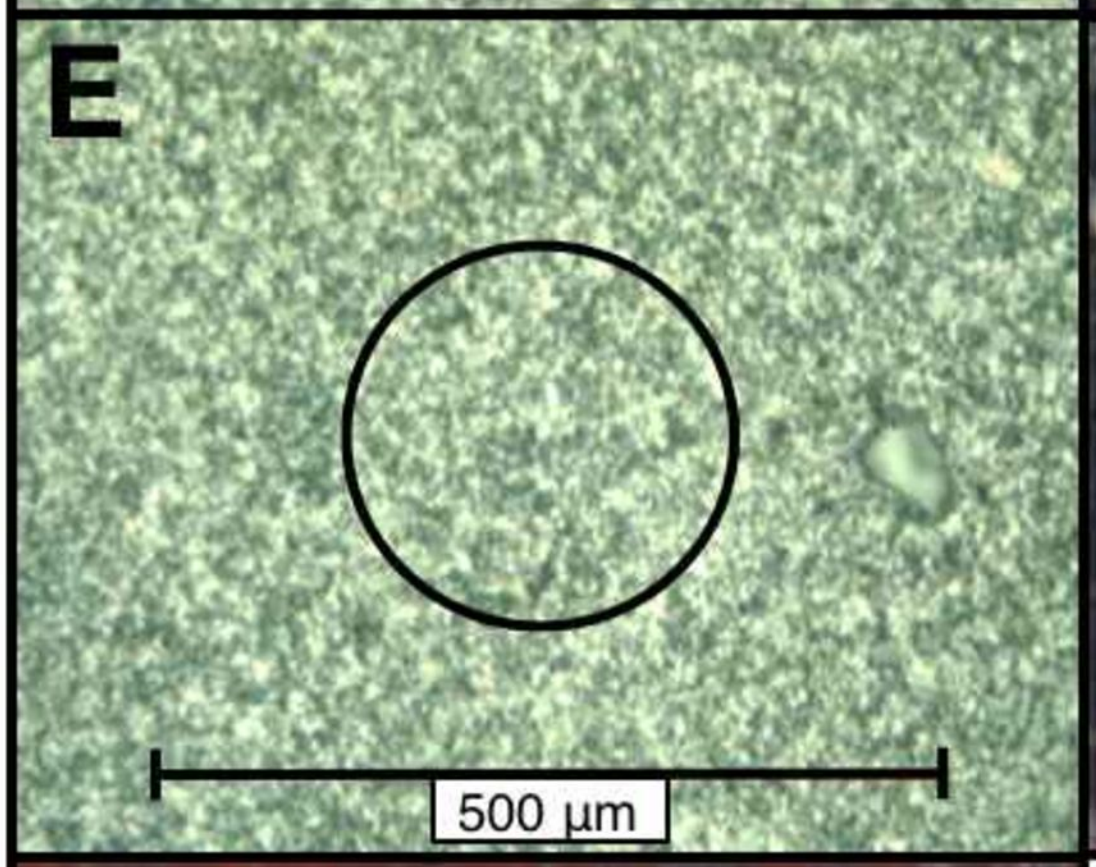

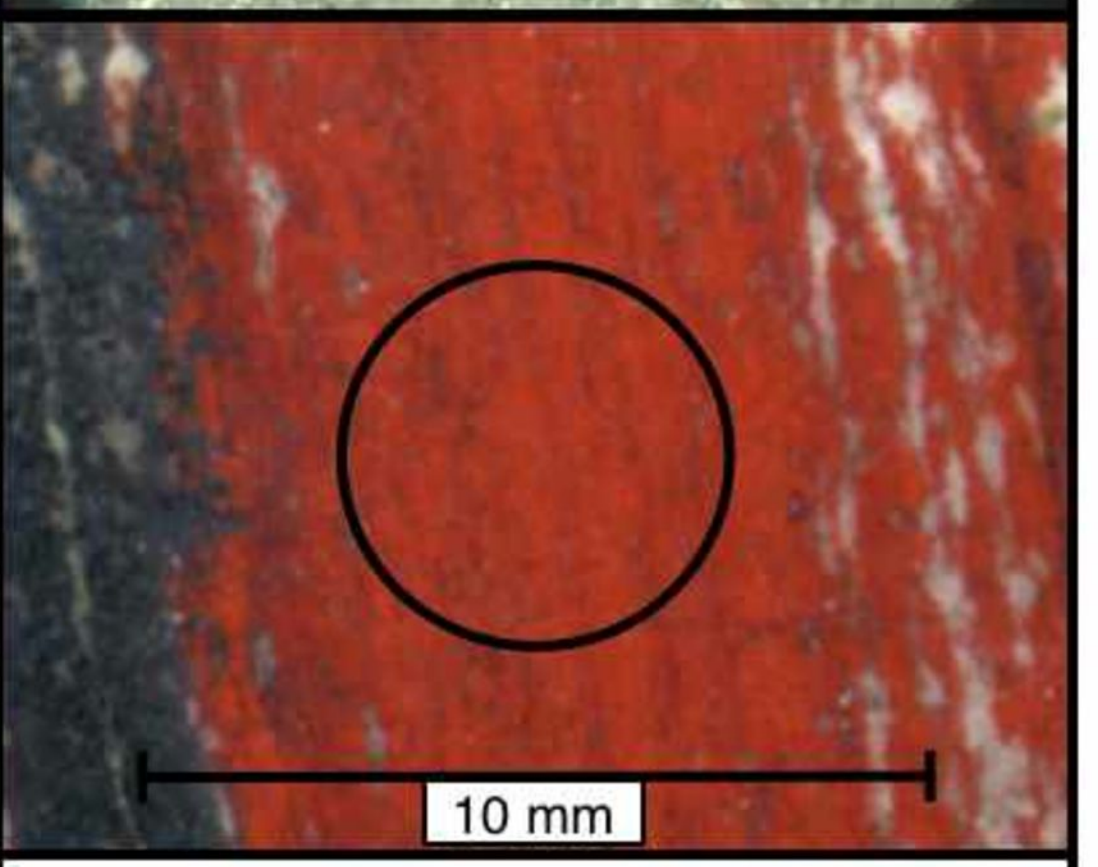

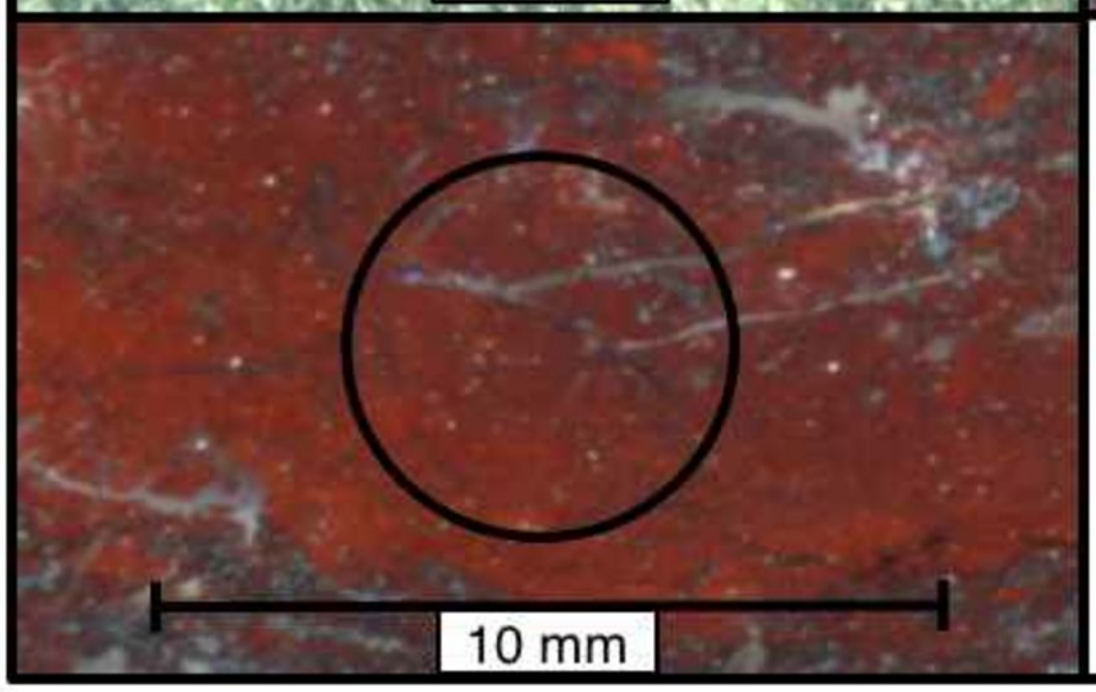

Circle ≈ 300 µm; ≈ 12 FTIR pixels

A) Moganite (solid);
Moganite, mixture (dashed)
B) Rose Chalcedony, moganite (solid);
Rose Chalcedony, no moganite (dashed)
C) Chalcedony (solid);
D) Chert
E) Novaculite
F) BIF
G) Jaspilite

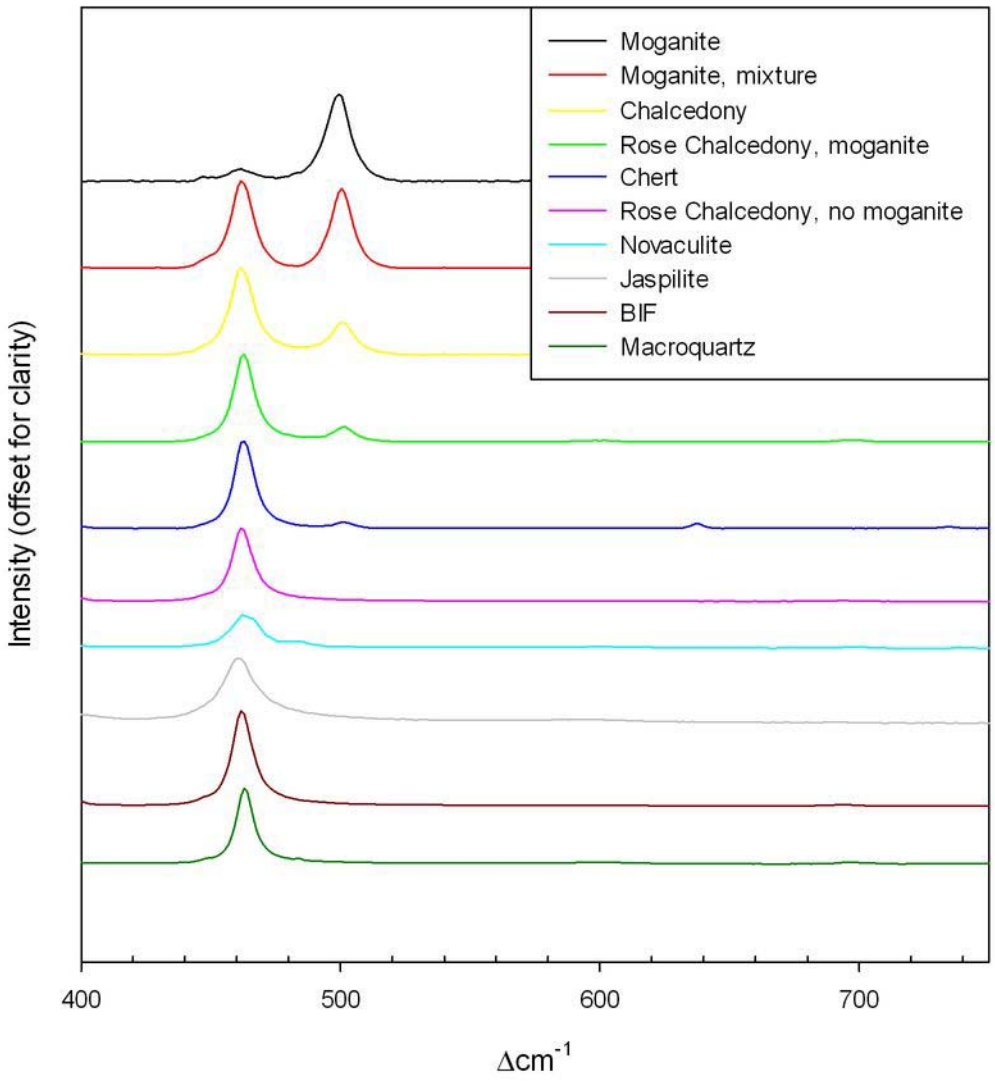
Moganite
Moganite, mixture
Chalcedony
Rose Chalcedony, moganite
Chert
Rose Chalcedony, no moganite
Novaculite
Jaspilite
BIF
Macroquartz
Intensity (offset for clarity)
400
500
600
700
Δcm-1

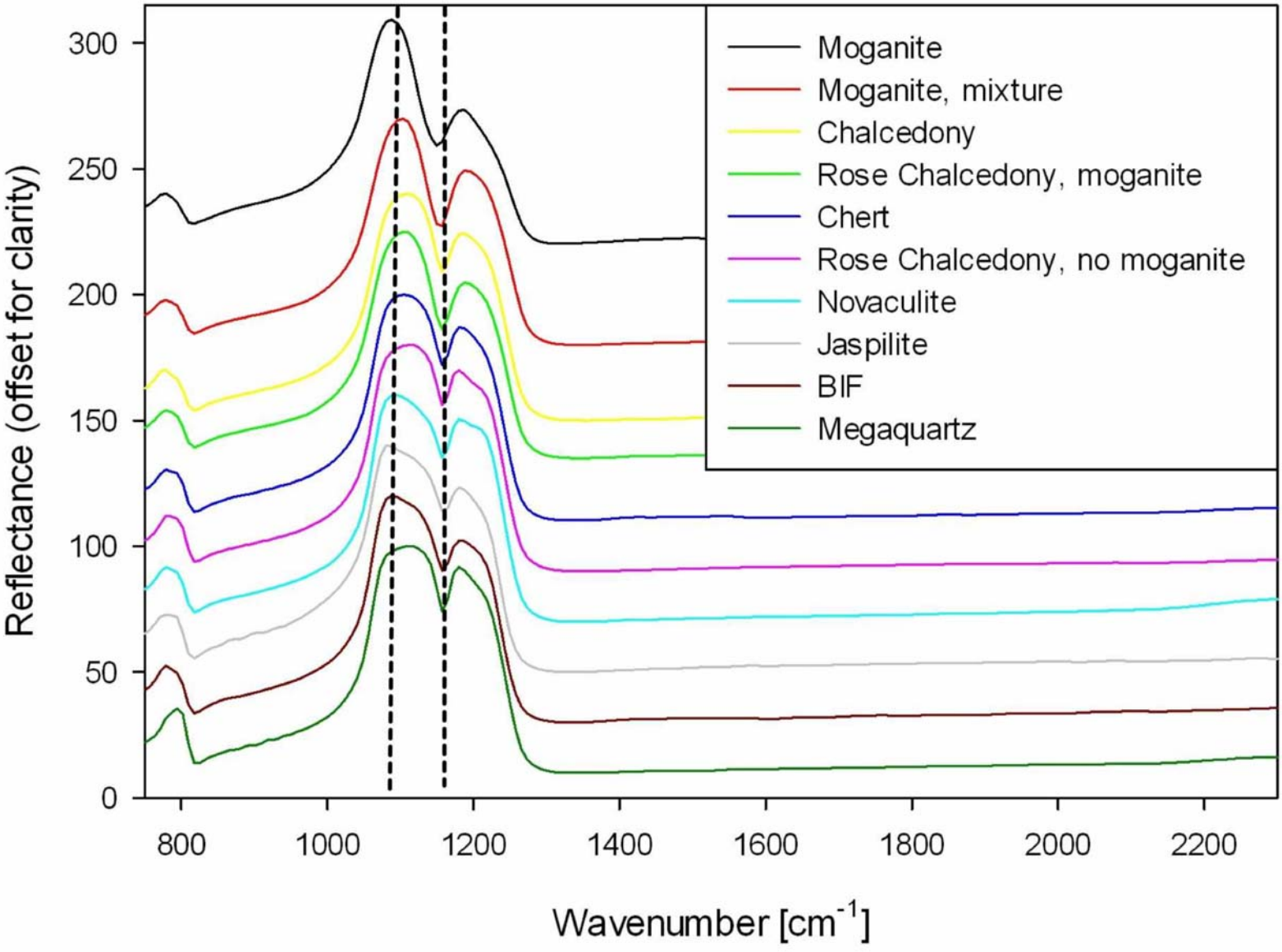
Moganite
Moganite, mixture
Chalcedony
Rose Chalcedony, moganite
Chert
Rose Chalcedony, no moganite
Novaculite
Jaspilite
BIF
Megaquartz
Reflectance (offset for clarity)
0
50
100
150
200
250
300
800
1000
1200
1400
1600
1800
2000
2200
Wavenumber [cm-1]

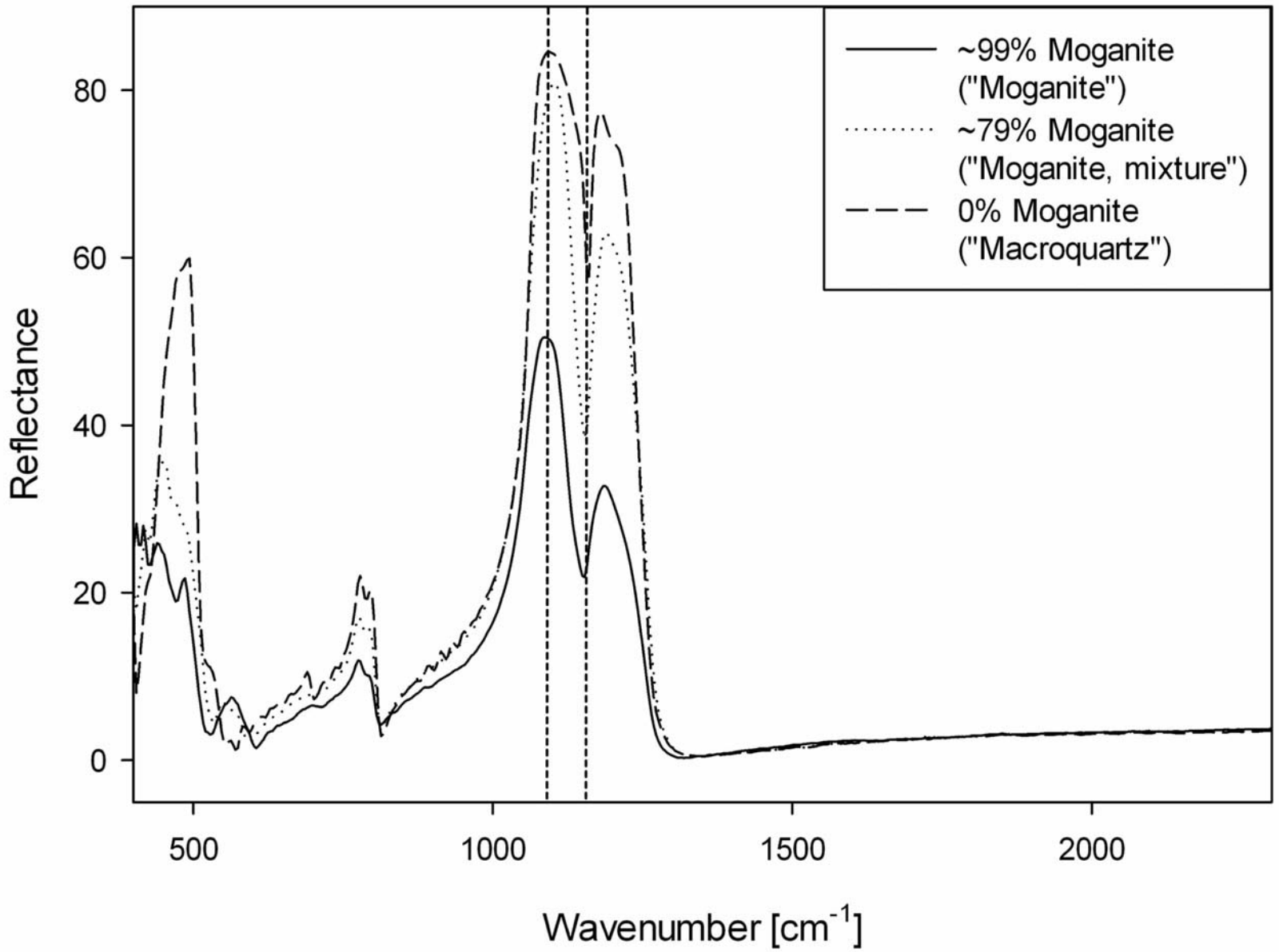
~99% Moganite
("Moganite")
~79% Moganite
("Moganite, mixture")
0% Moganite
("Macroquartz")
Reflectance
0
20
40
60
80
500
1000
1500
2000
Wavenumber [cm-1]

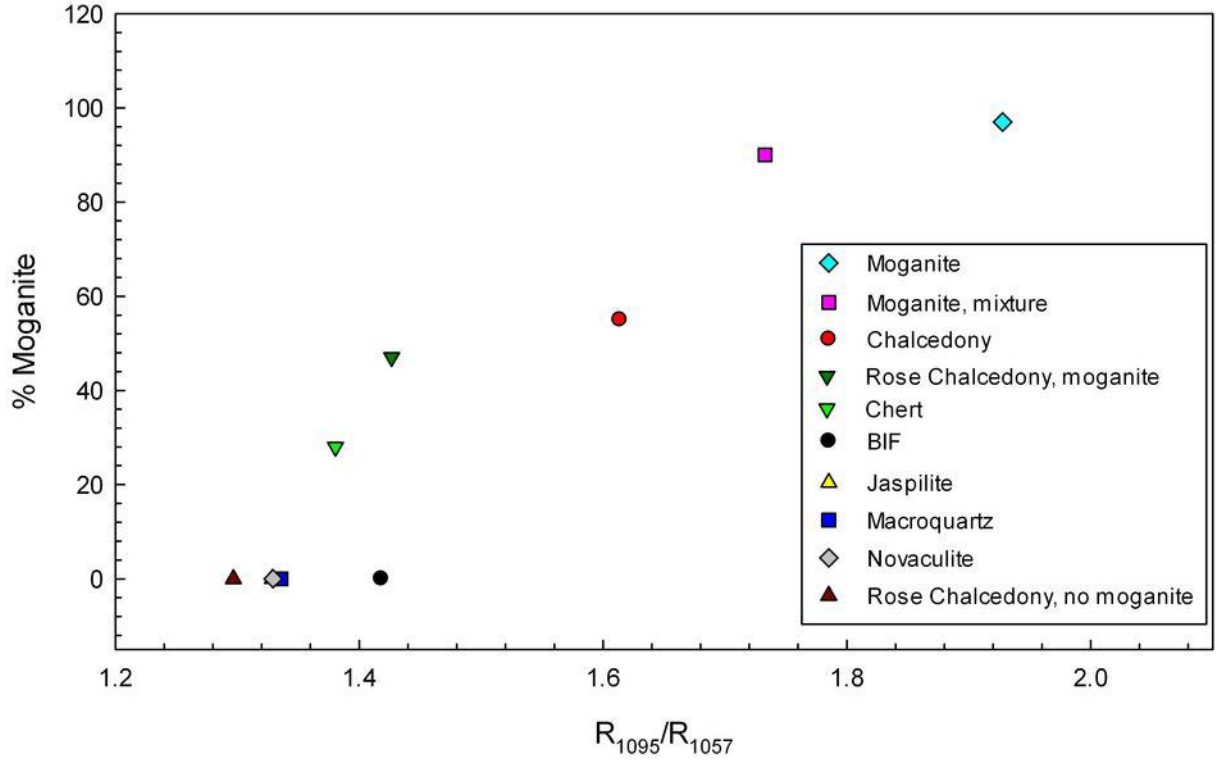
120
100
80
60
40
20
0
% Moganite
1.2
1.4
1.6
1.8
2.0
R_{1095}/R_{1057}
Moganite
Moganite, mixture
Chalcedony
Rose Chalcedony, moganite
Chert
BIF
Jaspilite
Macroquartz
Novaculite
Rose Chalcedony, no moganite

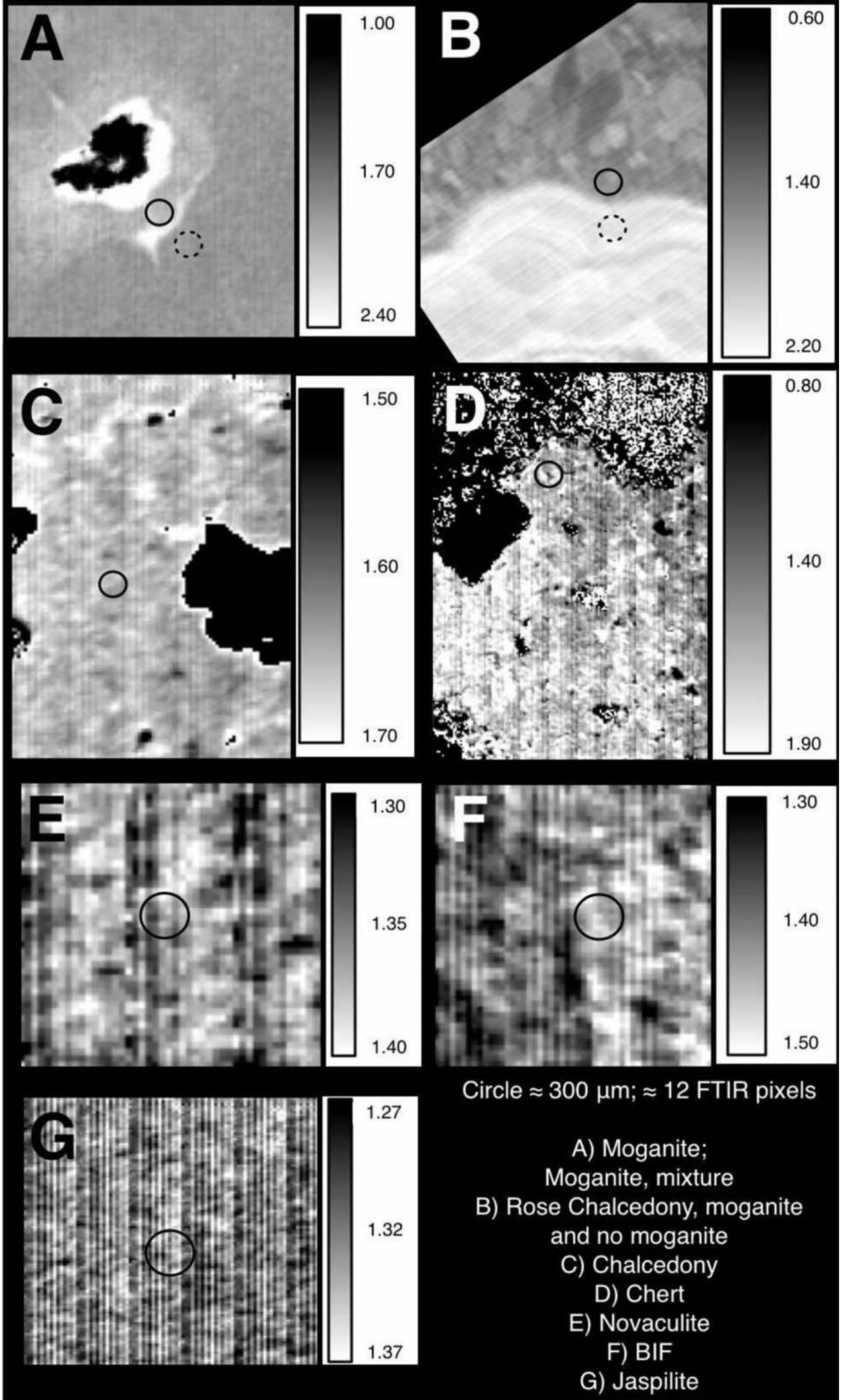
A
1.00
1.70
2.40
B
0.60
1.40
2.20
C
1.50
1.60
1.70
D
0.80
1.40
1.90
E
1.30
1.35
1.40
F
1.30
1.40
1.50
G
1.27
1.32
1.37
Circle ≈ 300 µm; ≈ 12 FTIR pixels
A) Moganite;
Moganite, mixture
B) Rose Chalcedony, moganite
and no moganite
C) Chalcedony
D) Chert
E) Novaculite
F) BIF
G) Jaspilite